Crack closure mechanisms in residual stress fields generated by laser shock peening

Keller, Sören; Horstmann, Manfred; Kashaev, Nikolai; Klusemann, Benjamin

Published in:
Engineering Fracture Mechanics

DOI:
10.1016/j.engfracmech.2019.106630

Publication date:
2019

Document Version
Publisher's PDF, also known as Version of record

Engineering Fracture Mechanics 221 (2019) 106630

Contents lists available at ScienceDirect

Engineering Fracture Mechanics

journal homepage: www.elsevier.com/locate/engfracmech

Crack closure mechanisms in residual stress fields generated by laser shock peening: A combined experimental-numerical approach

S. Keller[a,*], M. Horstmann[a], N. Kashaev[a], B. Klusemann[a,b]

[a] Helmholtz-Zentrum Geesthacht, Institute of Materials Research, Materials Mechanics, Max-Planck-Straße 1, 21502 Geesthacht, Germany
[b] Leuphana University of Lüneburg, Institute of Product and Process Innovation, Universitätsallee 1, 21335 Lüneburg, Germany

ARTICLE INFO

Keywords:
Laser shock peening
Residual stress
Fatigue crack growth
Crack closure
Stress intensity factor

ABSTRACT

Laser shock peening (LSP) is successfully applied to retard fatigue cracks in metallic lightweight structures by introducing specific, in particular compressive, residual stress fields. In this work, experiments and a multi-step simulation strategy are used to explain the fatigue crack retarding and accelerating mechanisms within these LSP-induced residual stress fields. Crack face contact is identified as main mechanism to retard the fatigue crack as the stress distribution changes and the stress intensity factor range decreases. Crack face contact is experimentally detected by load vs. crack opening displacement (COD) curves and scanning electron microscopy (SEM) of the crack faces, as well as during numerical simulations. The convincing agreement between experiment and simulation, especially regarding the specific crack face contact areas, allowed the proper evaluation of the stress intensity factors depending on the crack length. It is found that crack closure is indeed one of the main reasons for the efficient application of LSP for fatigue crack retardation. Furthermore, the occurrence of crack closure does not indicate a zero value stress intensity factor in complex residual stress fields, as the areas of crack face contact depend strongly on the LSP-induced compressive residual stresses.

1. Introduction

Understanding the influence of residual stresses on the fatigue crack propagation (FCP) of long cracks is important for a damage-tolerant design, e.g. applied for the fuselage of an airplane [1]. While manufacturing processes like welding introduce high tensile residual stresses in the weld zone, which might accelerate the fatigue crack growth [2], local modification techniques such as laser shock peening (LSP), shot peening, and rolling, introduce purposefully compressive residual stresses in the area where the surface modification techniques are applied. LSP combines a relative high penetration depth and surface quality [3] with excellent process controllability. These characteristics make the LSP process suitable for defined modifications of residual stress fields. Compressive residual stresses are locally introduced to reduce the crack driving load at the fatigue crack tip. Independently of the process, which is used to modify the residual stress field in any component, tensile residual stresses are always induced as well. Hence, the knowledge of the overall introduced residual stress field is mandatory to apply residual stress modification techniques most efficiently. Additionally, the fatigue retarding and accelerating mechanisms have to be understood as well.

Paris and Erdogan [4] were the first to link the change of the stress intensity factor to the FCP rate, which is generally known as Paris' law. Nowadays, the NASGRO equation [5] is often used, leading to an improvement in the FCP rate prediction, as the threshold regime, fracture toughness regime, and the mean stress effect of the stress intensity factor are considered. Keller et al. [6] showed that

* Corresponding author.
E-mail address: soeren.keller@hzg.de (S. Keller).

https://doi.org/10.1016/j.engfracmech.2019.106630
Received 14 March 2019; Received in revised form 19 July 2019; Accepted 16 August 2019
Available online 30 September 2019

Nomenclature

Acronyms

CCT	crack closure technique
COD	crack opening displacement
C(T)	compact tension
FCP	fatigue crack propagation
FE	finite element
LSP	laser shock peening
Nd:YAG	neodymium-doped yttrium aluminium garnet
SEM	scanning electron microscope
UP	unpeened

Symbols

a	crack length
C_{NA}	parameter of the NASGRO equation
f_N	Newmans crack opening function
F_{appl}	applied force
F_{op}	crack opening force
K_{appl}	stress intensity factor resulting from the applied loading only
K^*_{appl}	difference between K_{cd} and K^*_{res}
K_{cd}	stress intensity factor at the crack tip resulting from the combined stress state (residual and applied stresses) considering crack face contact
K_{res}	difference between K_{tot} and K_{appl}
K^*_{res}	stress intensity factor resulting from residual stresses only considering crack face contact
K_{tot}	stress intensity factor resulting from the superposition principle
N	number of load cycles
n_{NA}	exponent of the NASGRO equation
R_{cd}	crack driving stress intensity factor ratio
R_{Load}	ratio of the applied forces
u_y	displacement in y-direction
x_1, x_2	x-coordinates of the borders of the LSP-treated area
ΔK_{cd}	crack driving stress intensity factor range
$\boldsymbol{\varepsilon}_P$	plastic strain tensor
$\boldsymbol{\varepsilon}_{th}$	thermal strain tensor
$\boldsymbol{\sigma}$	stress tensor
σ_Y	yield strength of the material

the FCP rate influenced by LSP-generated residual stresses within AA2024-T3 sheet material can be predicted based on a multi-step finite element (FE) simulation approach calculating the crack driving stress intensity factor and subsequently applying the NASGRO equation. The predicted FCP rates agree well with the experimental test results. This finding is validated by a so-called 'experimental simulation', where the numerically determined crack driving stress intensity factor range ΔK_{cd} and ratio R_{cd} were experimentally applied to an unpeened specimen. The good agreement of the measured FCP rate by the 'experimental simulation' as well as by an experiment with a peened specimen verifies the calculated crack driving quantities. Hence, the question regarding the fatigue crack retardation and acceleration mechanisms is tackled in this work by investigating the phenomena which change the fracture mechanical crack driving quantities (ΔK_{cd} and R_{cd}) influenced by stresses from applied loads and residual stresses. This is addressed by a combined experimental-numerical approach.

2. Experimental techniques and theoretical principles

2.1. Laser shock peening

LSP is a surface treatment that is used to introduce compressive residual stresses in the target material. Short-time high-energy laser pulses are used to vaporize the target material surface. Caused by the energy input, the material is turned into plasma and expands rapidly, see Fig. 1(a). The expanding plasma causes a surface pressure at the solid target material, which introduces a mechanical shock wave into the workpiece [7]. The mechanical shock wave deforms the material plastically. Residual stresses remain in the specimen after the system reaches equilibrium. LSP leads to a characteristic residual stress distribution over depth, where high compressive residual stresses next to the surface decrease and might turn into tensile residual stresses next to the mid–thickness of the sheet material as shown by Chahardehi et al. [8], however, through depth compressive residual stresses are achievable for thin sheets as well, see [9]. Furthermore, the in–surface plane residual stress components can be influenced by certain laser shot sequences and energies [10]. While residual stresses are the focus of this work, a review of further possible surface enhancements based on an LSP treatment is provided by Clauer and Lahrman [11].

In this work, LSP is applied at a distance of 10 mm in front of an initial fatigue crack in 4.8 mm thick C(T) specimens with a width of 100 mm of AA2024-T3. AA2024 is typically used in the aircraft industry for fuselage structures due to the very good resistance to FCP and, therefore, very good damage tolerance properties [12]. The sheet material contains a clad layer at the surfaces with approximately 0.15 mm thickness. Water is used as confinement overlay to increase the efficiency of the LSP process.

An Nd:YAG laser was used, where the laser parameters, in particular the 20 ns laser pulse duration (full width at half maximum), the 5 J laser pulse energy, and the 3×3 mm^2 square focus, were kept constant. The laser pulses were shot in sequences, where the pulses are placed next to each other without overlap of the radiated areas of each pulse in columns. An area of 15×80 mm is peened by this pattern, as shown in Fig. 1(b). The pattern is shot twice on each surface side, which is named two-sided LSP treatment.

2.2. Fatigue crack propagation

The FCP rate was measured using C(T) specimens which were pre-cracked to the crack length of 25 mm and subsequently treated by LSP. The FCP test was conducted in air at room temperature. The specimens were tested under constant amplitude loading. The

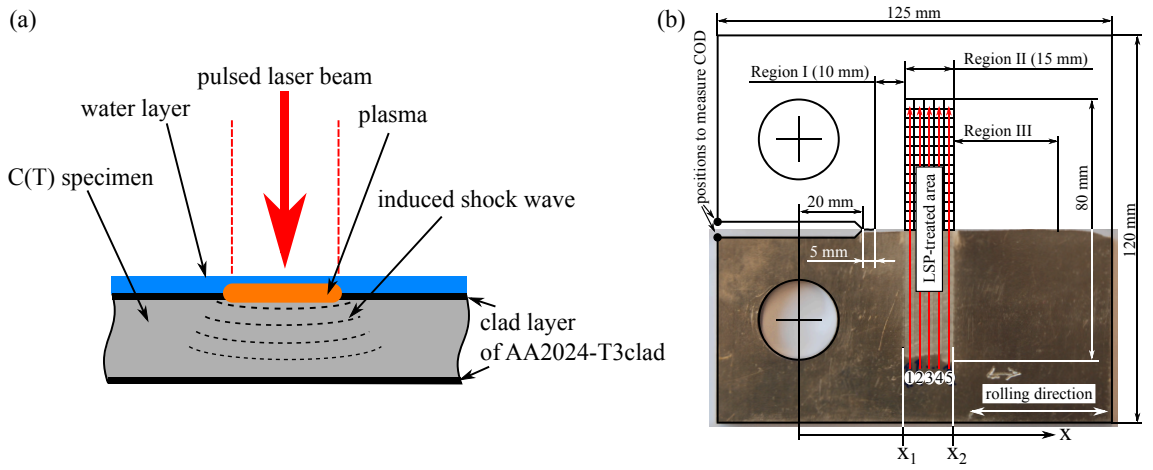

Fig. 1. Schematic of the LSP process (a) and the C(T) specimen consisting of a photo and a drawing (b). 5 J laser pulses with a duration of 20 ns (full width at half maximum) with a square focus size of 3 × 3 mm were shot onto the C(T) specimen. The laser pulses were shot without any overlap. The LSP pulse pattern is shot twice on both sides on the C(T) specimen (b).

load ratio

$$R_{Load} = \frac{F_{appl,min}}{F_{appl,max}} \tag{1}$$

is defined by the applied minimum and maximum forces $F_{appl,min}$ and $F_{appl,max}$, respectively. Specimens were tested with $R_{Load} = 0.1$ and $R_{Load} = 0.7$, both with the maximum applied load $F_{appl,max} = 4000$ N. The crack length was measured with optical microscopy from both sides of the specimen. The crack length is determined as the average distance between the applied load lines (origin of the coordinate x, see Fig. 1)) and the location of the measured crack tip from both specimen sides at the surface. In the following, the C(T) specimen is separated into three different regions, indicated by x_1 and x_2, to describe the FCP behaviour precisely, see Fig. 1(b)[1].

Region I $x < x_1$; The region between the initial crack tip and the peened area.
Region II $x_1 < x < x_2$; The region of the peened area.
Region III $x_2 < x$; The region behind the peened area.

2.3. Stress intensity factors and crack closure

We assume that the actual stress state is present when external loads and residual stresses act simultaneously. Typically, a superposition principle is applied, where the total stress intensity factor K_{tot} is used as stress intensity factor of the actual stress state. K_{tot} is separated into the applied stress intensity factor K_{appl} and the residual stress intensity factor K_{res}; $K_{tot} = K_{appl} + K_{res}$. The assumption that K_{appl} and K_{res} can be calculated by applying external loads and residual stresses separately, as used in [13,14], is described as traditional superposition in the following. Crack closure effects occur under high compressive residual stresses even at applied tensile loads. These crack closure effects lead to an error of the calculation of K_{tot} when the traditional superposition principle is applied [13] leading to the question of the physical meaning of K_{appl} and K_{res} in case of crack closure.

Consequently, in this paper a different definition of the stress intensity factors caused by applied loads and residual stresses is used to simplify the physical understanding. Corresponding to the meaning of 'residual stress', the remaining stress intensity factor after the removal of all external loads is named 'residual stress intensity factor' K^*_{res}. The applied stress intensity factor K^*_{appl} is the difference of the actual stress intensity factor K_{cd} and K^*_{res}

$$K^*_{appl} := K_{cd} - K^*_{res}. \tag{2}$$

In the context of this current work, the actual stress intensity factor K_{cd} is named crack driving stress intensity factor. Definition (2) implies that the applied stress intensity factor K^*_{appl} depends on the residual stress state at the crack tip. The crack driving stress intensity factor range ΔK_{cd} and the crack driving stress intensity factor ratio R_{cd} are determined as follows:

$$\Delta K_{cd} = K_{cd,max} - K_{cd,min}, \qquad R_{cd} = \frac{K_{cd,min}}{K_{cd,max}}. \tag{3}$$

Three different cases should be distinguished depending on the presence of residual stresses and its interaction to the applied

[1] $x_1 = 35$ mm includes 20 mm length of the initial notch, 5 mm length of the pre–crack, and 10 mm distance between the peened area and the pre–crack; $x_2 = 50$ mm includes x_1 and 15 mm length of the peened area.

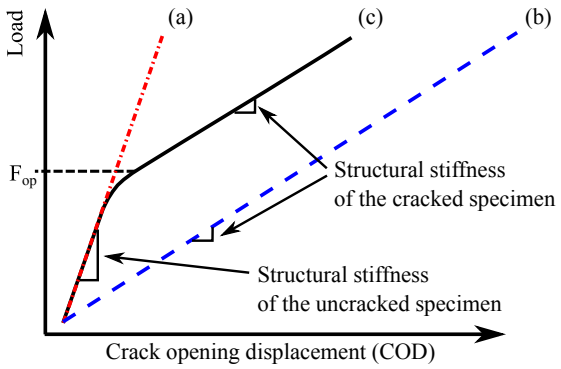

Fig. 2. Idealized load vs. crack opening displacement (COD) curve for an uncracked specimen (a), a cracked specimen (b), and a cracked specimen with crack closure (c). The stiffness of the specimen decreases with an increasing crack length, compare (a) and (b). F_{op} indicates the highest load where crack closure occurs during a load cycle.

loads.

Case 1 No residual stresses occur, the stress intensity factor can be calculated by an equation depending on the specimen geometry, the crack length, and the externally applied load, e.g. for C(T) specimens ASTM E647-11.
Case 2 Significant residual stresses are present and the traditional superposition principle [15–17] can be applied, as the crack is completely open.
Case 3 Significant residual stresses are present, but the traditional superposition principle cannot be applied due to crack closure.

Case 3 is characterized by crack closure leading to a change in the stress distribution, resulting in significant changes of ΔK_{cd} and R_{cd}. Assuming given residual stresses along the crack, the occurrence of crack closure depends on the applied external loading. Hence, the stress distribution and K^*_{appl} are influenced by the areas of crack face contact defined by the residual stresses and the applied loads. This leads to different K^*_{appl} if the residual stress field changes; however, the applied loads remain constant.

Elber [18] first developed a crack opening function for untreated material taking crack closure into account. Crack closure within untreated material is understood as result of a plastic wake caused by the previous plastic zone at the crack tip. In this work, a similar effect of LSP on the FCP rate is observed. LSP causes plastic deformation, resulting in residual stresses in the uncracked material. The separation of the material by the growing fatigue crack leads to deformation of the crack surfaces. Compressive residual stress areas in the uncracked material are supposed to be the areas of crack face contact in the cracked specimen. Hence, the areas of crack face contact depend on the individual residual stress distribution, resulting from the LSP treatment. Therefore, a general crack opening function cannot be applied and an FE model is used to investigate the fatigue crack retarding and accelerating mechanisms after the LSP treatment. It must be noted that crack closure might be also influenced by the roughness of the crack surfaces and other physical phenomena [19], which are assumed to be not influenced by LSP.

2.4. Crack opening displacement

Crack closure can be detected experimentally by the load vs. crack opening displacement (COD) curves. COD was measured at the crack mouth of the initial notch using strain clips, as illustrated in Fig. 1(b). Commonly, applied load (ordinate) and COD (abscissa) curves are used to evaluate the structural stiffness of the specimen, which is determined by the gradient of the COD load curve, see Fig. 2. The knowledge of the structural stiffness finds application in the calculation of the crack length, as the structural stiffness decreases with increasing crack length. Applied load and COD relate linearly for an opened crack. In case of crack closure, the structural stiffness increases, as the crack length of the opened crack is decreased. The stiffness of an uncracked specimen corresponds to the structural stiffness of the specimen with a completely closed crack, see (a) and (c). Hence, a change in structural stiffness indicates that crack closure occurs during the load cycle. The force at the transition point where the structural stiffness changes is called opening force F_{op}, as a larger force guarantees a completely opened crack. To determine the load range at which crack closure occurs, at certain crack length selected load cycles with $R_{Load} = -1$ are applied ($F_{appl,max} = 1800$ N), see Section 4.2. It has to be mentioned, that buckling was not observed for negative load ratios R_{Load} due to the relatively thick specimens of 4.8 mm thickness. Furthermore, the measured FCP rate during the test did not differ from measured FCP rates of specimens tested without the application of the selected load cycles with $R = -1$. Specimens, which are tested with selected load cycles at $R = -1$ are not used for the investigation of the fracture surface in Section 4.2.4.

2.5. Scanning electron microscopy

Scanning electron microscopy (SEM) is characterized by high resolution, depth of focus as well as possibility of direct observation of specimens. Therefore, it was used to investigate the C(T) specimens fracture surfaces based on topography contrast. SEM (Jeol

JSM-6490L) was conducted with 25 keV high voltage, 71 μA emission current, 0.013 nA, 30 μm aperture and 20–22 mm working distance.

Fracture surfaces of fatigued AA2024-T3 specimens often exhibit numerous fracture paths, whereby height differences between the individual fracture paths can be present in case of ductile fatigue fracture. Height differences can be interpreted as degrees of local plastic strain. Furthermore, a fracture path reveals fatigue striations parallel to one another bounded by fatigue lines. The fatigue striations of individual fracture paths indicate the direction of fatigue crack propagation [20,21]. SEM is used to investigate the change in microscopic features of fracture surface to clarify the influence of the LSP treatment. While this work uses SEM to detect areas of crack closure, the fatigue striation spacing after LSP treatment is evaluated, e.g. by Sheng et al. [22] for the aluminium alloy 6061-T6 or by Sun et al. [23] for the titanium alloy Ti-17.

3. Simulation and FCP rate prediction

3.1. Multi-step simulation to predict the FCP rate

The calculation of the FCP rate is based on the multi-step simulation approach that is proposed, applied, and validated by Keller et al. [6]. This allows the prediction of the FCP rate influenced by the LSP-induced residual stresses. The multi-step simulation consists of four main steps, see Fig. 3, which are briefly discussed in the following.

3.1.1. Step 1: LSP process simulation

An LSP process simulation, as used in [24], is applied to predict the plastic strain ε_P after the LSP treatment. Principle of periodicity is assumed, allowing the calculation of the LSP-introduced plastic strains ε_P for a representative area only. These plastic strains are applied subsequently to a larger area, predicting the residual stresses in the C(T) specimen, see Section 3.1.2. The LSP process simulation consists of an area of 3 × 3 laser pulses applied from both sides of a modelled sheet. The laser sequence is shot twice at both sides. Thus, 36 laser impacts need to be simulated in total.

The LSP process simulation consists of a shock wave propagation step and a relaxation step. An elastic–viscoplastic material model is employed where the rate–dependent plastic material behaviour is modelled using the Johnson–Cook model [25]. Pressure loading is applied at the target surface to simulate the laser pulse impact. The pressure pulse for 5 J laser pulses and 3 × 3 mm^2 laser focus are taken from [24].

3.1.2. Step 2: Eigenstrain transfer

The determined plastic strains of the LSP process simulation are transferred to the FE model of a C(T) specimen. This strain transfer is realized using the eigenstrain method. To this end, the simulated sheet of the LSP process simulation is partitioned into small volumes. The plastic strains of each volume are averaged component-wise. Accordingly, the LSP-treated area of the modelled C(T) specimen is partitioned into volumes with the same size. Each volume of the C(T) specimen is assigned to a volume of the LSP process simulation based on the assumption of periodicity. The averaged plastic strain components of the LSP process simulation are then introduced in the C(T) specimen as thermal strains by the allocation of anisotropic thermal expansion coefficients with a corresponding temperature increase. The different areas of thermal strains lead to elastic distortions of the system, which cause the intended residual stress distribution. The applied temperature is kept constant during Step 3 to include the effect of residual stresses in the stress intensity factor calculation. The small thickness (0.2 mm) in z-axis direction of the volumes guarantees a high resolution

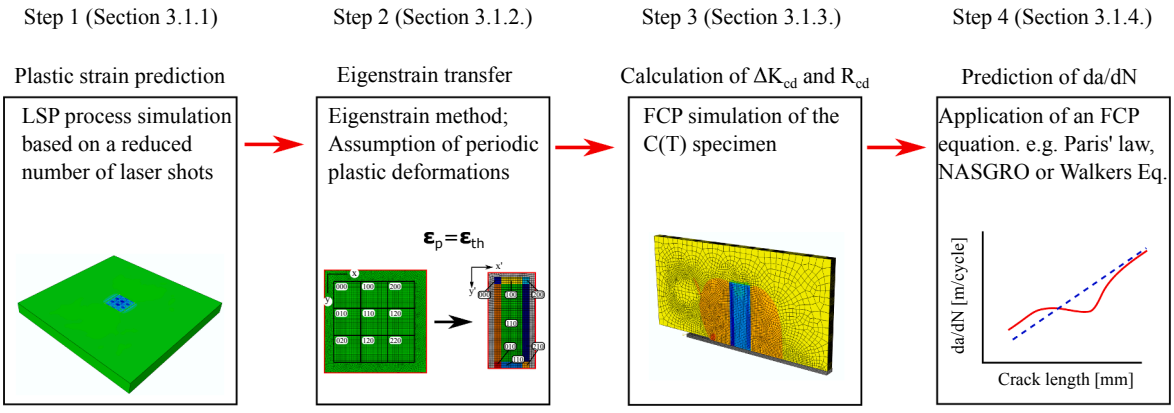

Fig. 3. Multi-Step simulation strategy to predict the FCP rate. First, the plastic strains resulting from LSP treatment are predicted based on an LSP process simulation. Second, the predicted plastic strains are introduced to the larger area of the C(T) specimen as thermal strains. Third, the prediction of the residual stress field and the stress intensity factors for different crack lengths in the C(T) specimen are presented. Finally, the FCP rate based on the calculated stress intensity factors and the NASGRO equation is predicted. Figures reprinted from [6], under the terms of the Creative Commons Attribution-NonCommercial-NoDerivatives 4.0 International (CC BY-NC-ND 4.0). https://creativecommons.org/licenses/by-nc-nd/4.0/.

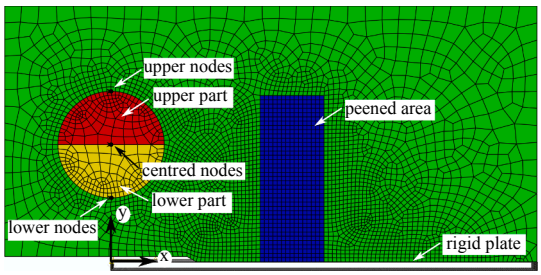

Fig. 4. Three-dimensional FE model of the C(T) specimen. The crack is extended step–wise according to the element size. The position of the external forces is chosen depending on the quantity, which has to be predicted (stress intensity factor: see Section 3.1.3 or load vs. COD curves: see Section 3.2).

of the residual stress gradient perpendicular to the surface. However, the residual stress field does not show the high fluctuation parallel to the target surface of the LSP process simulation as the applied averaging scheme neglects this stress fluctuation.

3.1.3. Step 3: Prediction of the crack driving quantities via FCP simulation

Half of the C(T) specimen is modelled considering symmetry, see Fig. 4. The spatial mesh discretization guarantees a sufficiently high resolution of the residual stresses in depth direction as well as a mesh-independent solution. The material behaviour during the FCP simulation is modelled as linear elastic. The force of the FCP test is applied as a distributed force at the centred nodes of the bolt. The bolt is divided into two parts, where the upper part contains a high and the lower part a reduced stiffness to guarantee the load transfer of the applied force through the upper part of the bolt. The bolt is merged with the C(T) specimen avoiding contact modelling. This load application scheme leads to predictions of the stress intensity factor in a good agreement with experimental tests, as shown in Keller et al. [6]. Please note that the load is applied differently for the prediction of the load vs. COD curves, see Section 3.2, since perfectly bonded bolts mimic unphysical high friction.

The crack driving stress intensity factor range ΔK_{cd} and ratio R_{cd} are calculated based on the crack closure technique (CCT) [26] assuming plane stress conditions. To model the crack growth, the nodes on the symmetry line are successively replaced by contact conditions to a rigid plate. This contact along the symmetry line simulates the contact of the crack faces in case of crack closure. The applied CCT calculates one stress intensity factor for the entire specimen thickness.

3.1.4. Step 4: Calculation of the FCP rate

Assuming that crack growth occurs in Paris' regime, according to [5] the FCP rate can be predicted using a reduced NASGRO Eq.

$$\frac{\mathrm{d}a}{\mathrm{d}N} = C_{NA}\left[\Delta K_{cd}\,\frac{(1-f_N)}{(1-R_{cd})}\right]^{n_{NA}}. \tag{4}$$

$C_{NA} = 4.435{\cdot}10^{-11}$ and $n_{NA} = 3.646$ are material parameters identified for the unpeened material, see Keller et al. [6]; f_N is the crack closure function found by Newman [27][2]. Keller et al. [6] showed that C and n, representing material specific constants, are not changed by the performed LSP treatment; hence, C_{NA} and n_{NA} are used for the prediction of the peened material as well.

In general three different sources of plastic deformation has to be considered during the stress intensity factor prediction. First, LSP generates plastic deformation, representing the eigenstrains, which are introduced to the C(T) specimen model. Second, plastic deformation is caused by the stress intensity. Considering a propagating fatigue crack a plastic wake along the crack surfaces is generated. The plastic wake is considered by the Newmans crack opening function in the NASGRO Eq. (4). A third source of plastic deformation may be contact forces between the crack surface during crack closure events. Investigation of simulations based on an elastic-plastic material behaviour of the C(T) specimen model showed, that these plastic deformation is relatively small and does not influence the calculated stress intensity factors significantly in the current case. Hence, the assumption of purely elastic material behaviour during Step 3 is found to be valid for the investigated residual stress fields.

3.2. Calculation of the load vs. COD curves

Load vs. COD curves are calculated based on the FE model of the C(T) specimen after Step 2, see Section 3.1.2. In contrast to Step 3 in the multi-step approach for predicting the crack driving quantities, for calculating the COD the force is applied as distributed load at the nodes at the top of the drilling in the C(T) specimen, as indicated in Fig. 4. The bolt is not explicitly modelled, to represent a sufficiently thin bolt with no contribution to the measured stiffness of the load vs. COD curve. This simplification reduces the numerical effort of the simulation as well, but neglects phenomena such as friction between bolt and specimen that could have an influence on the load vs. COD curve as shown by Johansson and Fitzpatrick [28].

The force is set to the value 1.8 kN and is reduced linearly to − 1.8 kN. COD is calculated from the node displacement (y-direction) from the nodes located at the crack mouth of the C(T) specimen, as shown in Fig. 1(b).

[2] Note that the yield strength σ_Y and the coefficient of the load state $\alpha = 3.0$ of the crack closure function were taken from Keller et al. [6].

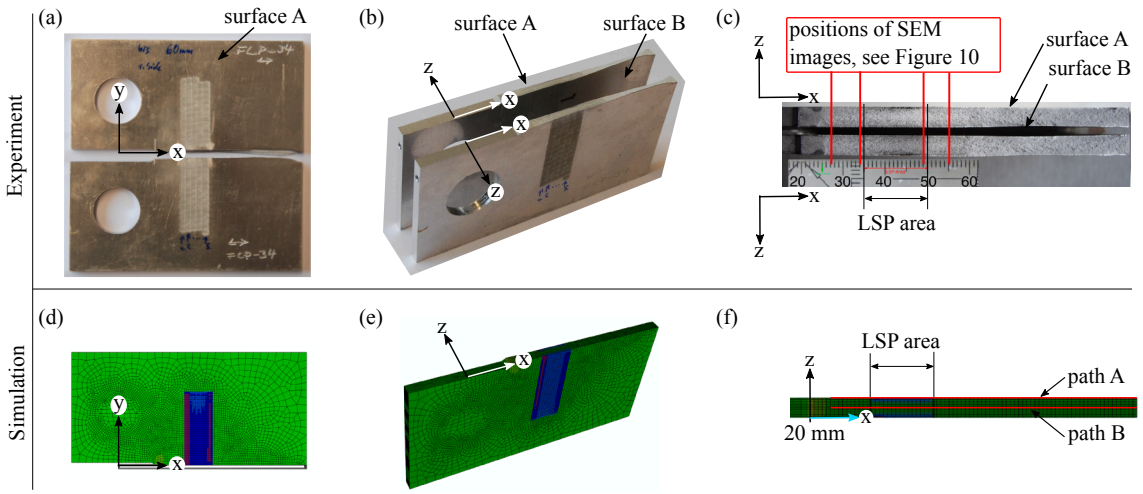

Fig. 5. Geometry of the C(T) specimen of the experiments (a–c) and of the FE simulation (d–f). The crack surface of the real specimen is studied using SEM at the four marked locations in the x-direction next to surfaces A and B, as well as next to mid–thickness, see Fig. 10. The residual stresses of the C(T) specimen model are evaluated along path A at the surface, along path B at mid-thickness, and at the crack front for different crack lengths, see Fig. 7.

The numerically determined crack opening force F_{op} is calculated by a Newton algorithm with the consideration of the entire fracture surfaces. Thus, the highest force at which crack face contact happens is accounted as F_{op} independently where the crack face contact is located along the crack surfaces.

4. Results and discussion

4.1. Evolution of residual stresses depending on the crack length

Residual stresses in the C(T) specimen change depending on the crack length. These changes are caused by the redistribution of the residual stresses when the crack cuts through the specimen. Liljedahl et al. [29] showed that redistributed residual stresses can be calculated with a purely elastic simulation, as plasticity does not have a major influence during redistribution. This observation is confirmed for the C(T) specimen model and the introduced residual stresses of this work. The changing residual stress distribution is visualized for different crack lengths of a C(T) specimen in Figs. 6 and 7.

Region I, the region in front of the peened area, is dominated by tensile residual stresses, which balance the compressive stresses of the peened area within the unloaded specimen. These tensile residual stresses occur throughout the thickness, see Fig. 7(c), and cause a stress intensity at the initial crack tip leading to $K^*_{res} > 0$.

Region II is defined by the size of the peened area. The specimen surfaces within Region II were treated via LSP; hence, compressive residual stresses are present next to the surface in the uncracked specimen. These near-surface compressive stresses cause balancing tensile stresses inside the specimen. The residual stress distribution over depth is characterized by a high spatial stress gradient, which is typical for LSP [8,24,30]. The balancing tensile residual stresses vanish at the crack edges if the crack tip is located in Region II as a result of the stress redistribution. Compressive residual stresses at the crack surfaces indicate the occurrence of crack closure, see Fig. 7(b) and (c). However, the residual stress intensity factor does not vanish over the thickness, as tensile residual stresses still cause a stress intensity in the centre of the specimen, see Fig. 7(a) and (c).

Region III is located behind the peened area and contains tensile residual stresses, balancing the compressive residual stresses located in Region II. Similar to the residual stress distribution of Region I, the tensile stresses are developed over the entire thickness of the specimen. Compared to Region I, the larger area of Region III where balancing tensile stresses are present leads to a reduced residual stress level at the crack tip after the crack reached Region III. Although the crack tip is located in Region III, compressive residual stresses at the crack edges in Region II indicate the occurrence of crack closure in Region II, see Fig. 7(b), which is also illustrated in Fig. 9.

4.2. Occurence and position of crack closure

Measured load vs. COD curves indicate F_{op} slightly below 0 kN for the unpeened specimen, where the numerical prediction gives $F_{op} = 0$ kN. This observation is consistent with the results of the peened specimens, where the simulation also predicts F_{op} slightly above the measured value. This shows a slight shift in the measurements to lower forces compared to the simulation due to the experimental set-up. However, it has to be mentioned that the experimentally determined F_{op} is very sensitive to numerous influences, such as the change of the loading condition through the bolt if the applied force changes the sign. Hence, the load vs. COD curves are not intended to be over-interpreted. Instead, this paper focus on qualitative changes between the peened and unpeend specimens

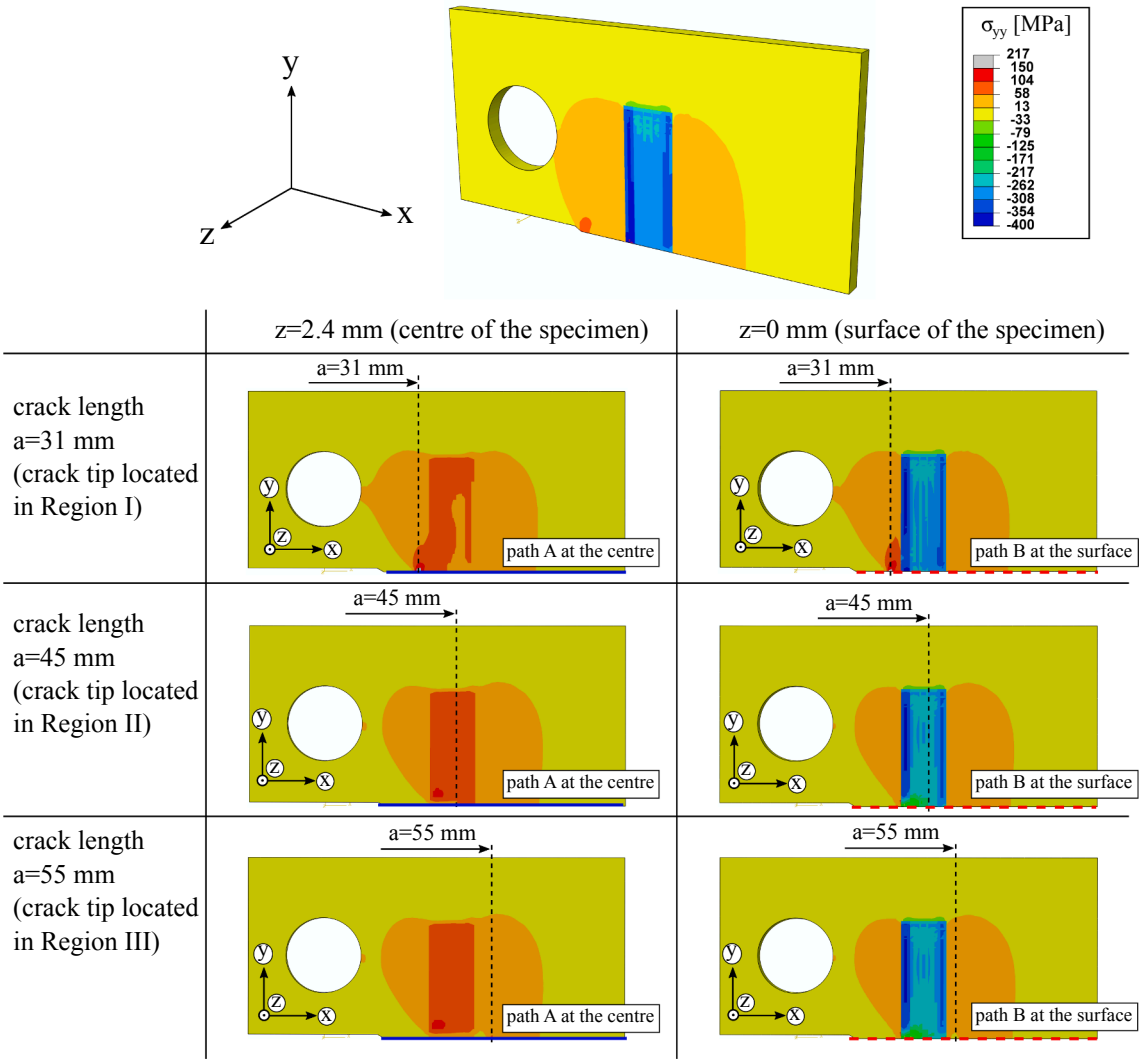

Fig. 6. Residual stress distribution of the peened C(T) specimen at the centre (left) and at the surface (right) at different crack lengths displayed. Paths A and B, depicted in Fig. 5, indicate where residual stresses are plotted in Fig. 7.

regarding experimentally determined load vs. COD curves. The stiffness of the C(T) specimen decreases with the increasing crack length for a completely opened crack. This decreasing stiffness can be observed for the unpeened specimens at loads higher than F_{op}, see Fig. 8(a) and (c). The stiffness for a closed crack corresponds to the stiffness of an uncracked specimen, as observed at loads lower than F_{op}. In case of the simulation of the unpeened specimen, the structural stiffness changes abruptly at $F_{op} \approx 0$ kN due to the undeformed plane crack edges. In contrast, the experimentally measured structural stiffness shows a smoother transition from the structural stiffness of the cracked specimen to the structural stiffness of the uncracked specimen. This is probably caused by a smooth crack closure in the experiment, which might result from surface roughness, or the plastic wake resulting from the previous plastic zone at the crack tip.

The shape of the load vs. COD curves of the peened specimens can be explained by specific regions of crack face contact. The positions where crack closure occurs, at the minimum load $F_{appl} = 0.4$ kN of the fatigue load cycle, are evaluated from the predicted displacement perpendicular to the crack edges, as shown in Fig. 9. Owing to surface roughness, the shape of the crack path, or plastic deformation at the crack surfaces in the experiment, crack closure might occur at slightly different loads in the experiments compared to the simulations.[3] The crack closure areas and the resulting load vs. COD curves will be discussed in the following.

4.2.1. Crack tip located in Region I

Peened specimens show a different behaviour compared to the unpeened specimens which is attributed to the introduced residual

[3] Recall, in the FCP simulations no plasticity, no surface roughness and a straight crack path are assumed.

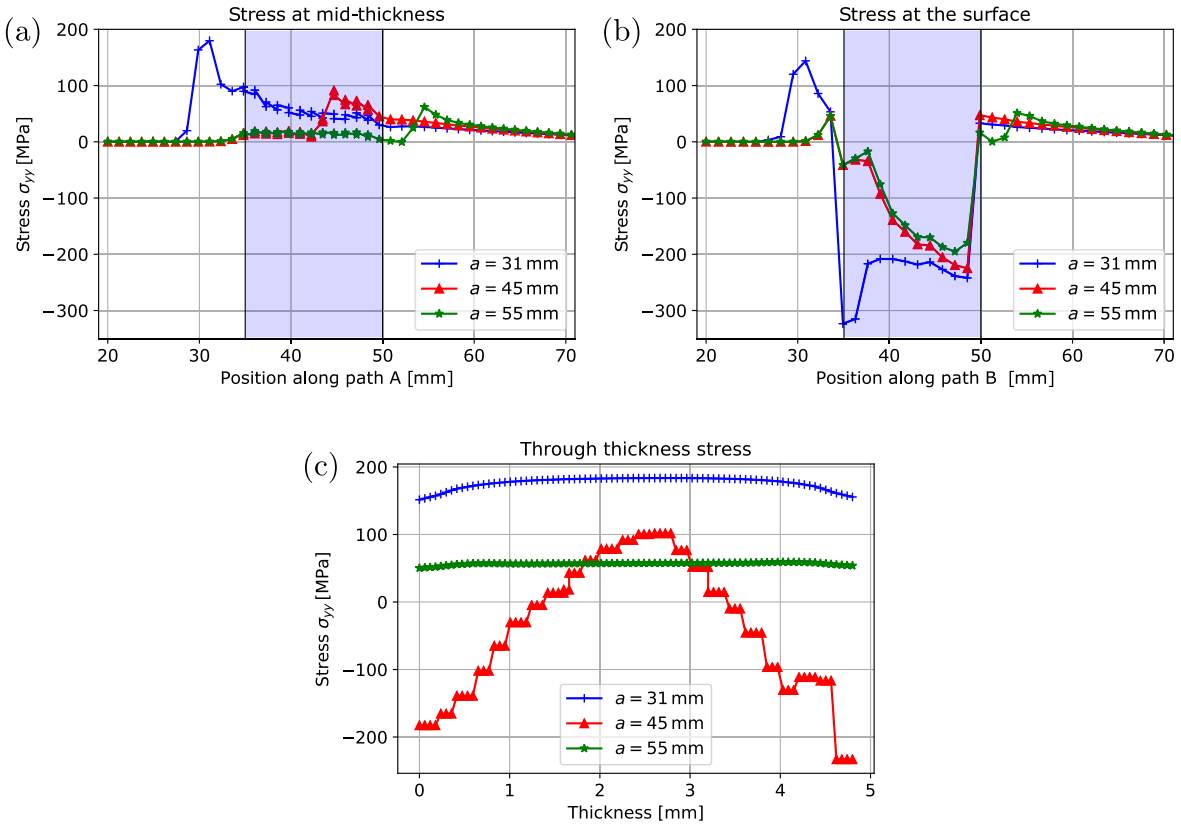

Fig. 7. Residual stresses for different crack lengths along the crack path (x-direction) next to mid–thickness of the C(T) specimen (a), at the surface (b), and along the crack tip (z-direction) (c). Paths A and B are depicted in Fig. 5.

stress field. Load vs. COD curves of small crack lengths, see Fig. 8 for $a = 31$ mm, representing Region I, do not show a change in the structural stiffness. However, since the stiffness of the peened specimen, Fig. 8(b), is lower compared to the stiffness of the unpeened and uncracked specimen, Fig. 8(a), this indicates an opened crack for the investigated load range. The simulation results, Fig. 8(c) and (d), confirm this observation and show that the permanently opened crack is caused by the tensile residual stresses of Region I, see Fig. 9(a).

4.2.2. Crack tip located in Region II

Both, measurement and simulation show a smooth change of the structural stiffness, where the stiffness at the minimum force does not reach the stiffness of the uncracked specimen, see $a = 45$ mm in Fig. 8(b) and (d). Region II contains the LSP generated compressive residual stresses. However, balancing tensile stresses are present at the centre of the specimen. The resulting stress gradient leads to crack closure next to the surfaces but not in the centre of the specimen at the minimum applied load if the crack tip reaches Region II, see Fig. 9(b). This LSP-induced crack closure causes the smoother change of structural stiffness compared to unpeened specimens, Fig. 8(a) and (c), as the crack does not close along the whole crack face. The higher F_{op} is also caused by the LSP treatment, as plastic deformation resulting by LSP are increasing the deformation of the crack edges in addition to the plastic wake. Furthermore, the structural stiffness remains constant for $F_{appl} < 0.5$ kN, which indicates that the position along the x-axis where crack closure occurs does not change if the applied force is decreased up to $F_{appl} = -1.8$ kN.

4.2.3. Crack tip located in Region III

The existence of crack face contact areas, which are not connected to the crack tip, explains the relatively high opening force F_{op} for large crack lengths, Fig. 8(c) and (d), while the FCP rate is still relatively high, see Keller et al. [6]. It is concluded that F_{op} cannot be related to the stress intensity factor without the exact knowledge of the areas of crack closure. The observation that the gradients of the load vs. COD curves remain constant for different crack lengths at low applied external loads (Fig. 8(b) and (d) $F_{appl} < 0$ N) in Regions II and III can be interpreted by similar crack face contact areas. In particular, the crack closes at similar locations independently of the current crack length, which are the areas next to the surface in the LSP-treated area, see Fig. 9(b) and (c).

4.2.4. Observation by SEM images

The results based on the load vs. COD curves coincide with observations using SEM images of the fracture surface, see Fig. 10. A tested peened C(T) specimen was separated into two pieces along the crack. SEM was used next to surfaces A and B, as well as at mid-

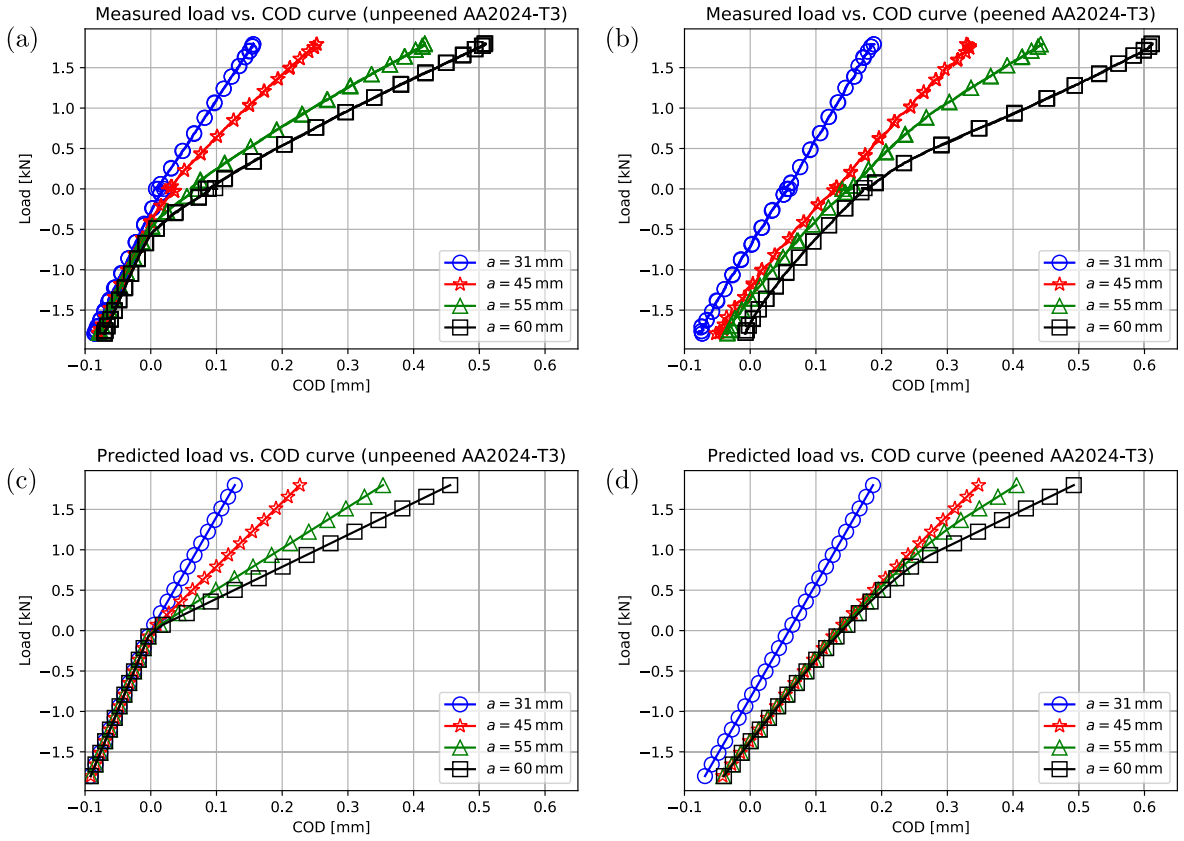

Fig. 8. Measured (a–b) and predicted (c–d) load vs. COD curves for different crack lengths for unpeened (a, c) and peened (b, d) C(T) specimens. The structural stiffness decreases with increasing crack length a. The change in the structural stiffness indicates the occurrence of crack closure effects for lower loads.

thickness to study the fracture surface at the marked positions, see Fig. 5. The outer regions as well as the interior area of the fatigue fracture surface were investigated at different positions: $x = 27$ mm, $x = 34$ mm, $x = 49$ mm and $x = 55$ mm. The micrograph at $x = 27$ mm shows fatigue striations parallel to one another bounded by fatigue lines. There are distinctions visible between the outer and inner region because of the clad layer of commercial pure Al at the surface. Bulk AA2024-T3 and the cladded aluminium deliver different appearances of fracture surface due to their microstructure regarding grain size and chemical composition. The numerous voids in the micrographs represent places of included Cu-rich particles. Between the micrographs at 27 mm and 34 mm the particular fracture surface regions show similar characteristics. A significant structure change has been determined at $x = 49$ mm. The fatigue fracture surface of AA2024-T3 next to the Al clad suffered plastic deformation through fretting of the crack surfaces leading to destruction of fatigue characteristics. The result is a locally flattened and low structured fracture surface due to crack closure. A similar plasticized fracture surface after LSP treatment was observed by Kashaev et al. [31]. The preserved fatigue characteristics in the cladded aluminium show that its structure was not significantly affected by crack closure due to tensile residual stresses in the clad layer preventing contact of the crack flanks.

The fracture surface in the centre at $x = 49$ mm, located in Region II, is comparable to the observed fracture surface in Region I. Thus, fatigue striations are visible, indicating that the fracture surface at mid-thickness is less affected by crack closure than the near surface area in Region II. This phenomenon is predicted by the FE simulations, which show tensile residual stresses that keep the crack open at mid-thickness and minimum load. Typical characteristics of a fatigue crack are observed in Region III throughout the depth, where no significant variations over the depth are present except for the clad layer. However, the higher loading caused by an increased stress intensity factor due to the long crack, $a > 50$ mm, changes the fracture surface slightly in comparison to Region I. It can be concluded that the fracture surface in Region III did not suffer more from crack closure compared to the near-surface area in Region II. This confirms the FE simulation-based predictions of the crack closure areas, see Fig. 9.

It is important to mention that the characteristic features detected by SEM were found consistently on both fracture surfaces and on different specimens.

4.3. Evolution of ΔK_{cd} and R_{cd} influenced by crack closure

The crack driving stress intensity factor range ΔK_{cd} and ratio R_{cd} of the peened specimen, as shown in Fig. 11, are predicted based

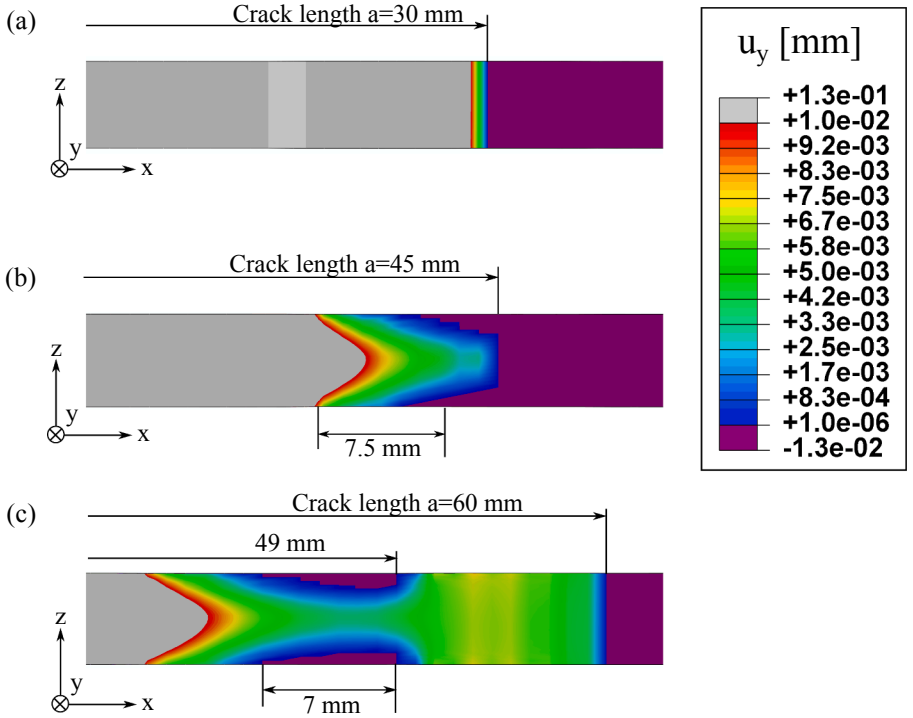

Fig. 9. Crack edges next to crack tip, as shown in Fig. 5, indicate the displacement u_y perpendicular to the crack plane for minimum applied load of 400 N. (a) The crack tip is in front of the peened area. (b) Crack tip within the peened area. Crack closure can be observed near the surface area where the compressive stresses are located. (c) The crack tip is behind the peened area. Crack closure occurs still in the peened area near the surface without connection to the crack tip.

on the multi-step simulation, see Fig. 3. Stress intensity factors of the unpeened specimen are calculated using ASTM E647-11.

If the crack tip is located in Region I, no crack closure is observed corresponding to Case 2, see Section 2.3. Tensile residual stresses open the crack and are superposed by the applied loads. The traditional superposition principle can be used to describe the stress intensity factor. The applicability of the traditional superposition principle can be seen in Fig. 11(c) where no differences between ΔK_{cd} of the peened and unpeened specimen are observed, in Region I. Consequently, differences of the FCP rate result only from the change in R_{cd}.

ΔK_{cd} and R_{cd} are highly influenced by crack closure when the crack tip is located in Region II, as described in Section 4.2. The fatigue crack growth in Region II belongs to Case 3. The occurrence of crack closure results in a reduction of ΔK_{cd}. A lower ΔK_{cd} leads to a significant retardation of the crack growth. Tensile stresses keep the crack tip opened in the centre of the specimen, leading to a minimum stress intensity factor $K_{cd,min} > 0\,\mathrm{MPa}\sqrt{\mathrm{m}}$. It can be observed that $K_{cd,min}$ of the peened specimen is most likely above $K_{cd,min}$ of the unpeened specimen and drops just in the crack range $45\,\mathrm{mm} < a < 50\,\mathrm{mm}$ slightly below this value. Hence, the assumption that crack closure reduces the minimum stress intensity factor cannot be justified for residual stresses showing a high gradient over the depth. R_{cd} drops in Region II, so that ΔK_{cd} is the main contribution to the resulting FCP rate.

The minimum and maximum stress intensity factors of the peened specimen converge against the stress intensity factors of the unpeened specimen behind the peened area, see Region III. While ΔK_{cd} of the peened specimen is reduced, R_{cd} is slightly increased compared to the unpeened specimen. The decreased ΔK_{cd} cannot be explained by the tensile residual stress at the crack tip, but with the observations of crack closure. Although the crack is already present in Region III, the crack still closes in Region II leading to Case 3. This crack closure influences the overall stress distribution compared to a completely opened crack. Therefore, the maximum stress intensity factor of the peened specimen remains below the maximum stress intensity factor of the unpeened specimen, although tensile residual stresses are present at the crack tip in Region III, see Fig. 7(c).

Stress redistribution due to crack face contact during the load cycles is assumed as the main phenomenon to reduce ΔK_{cd}. While R_{cd} dominates the crack propagation in front of the peened area, ΔK_{cd} is the main crack driving quantity within and behind the peened area.

4.4. Importance of crack closure and fast FCP rate prediction

To achieve an efficient application of LSP aiming at FCP retardation, it is important to introduce residual stresses which cause crack closure during the fatigue load cycle. This phenomenon can be illustrated by stress intensity factor vs. applied load curves, see Fig. 12, shown at three crack lengths to clarify the effect of residual stresses in each characteristic region. The relation between the

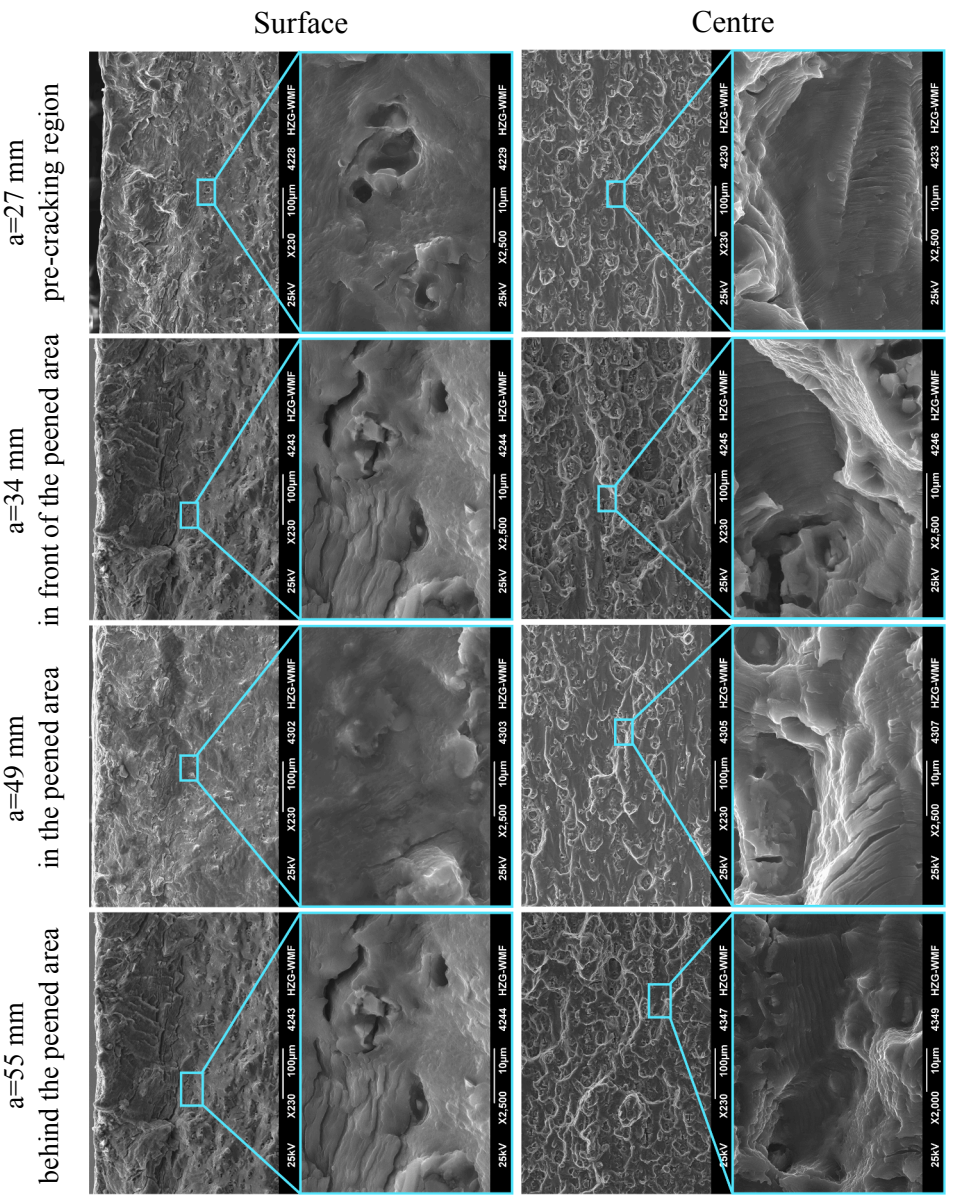

Fig. 10. SEM images of the fracture surface of a tested peened C(T) specimen. While the fracture surface in front of the peened area, $x = 27$ mm and $x = 34$ mm, as well as behind the peened area $x = 55.0$ mm, indicates characteristics of a fatigue crack though the depth, the surface next to the sheet–surface does not indicate this characteristic in Region II ($x = 49.0$ mm). The missing feature of a fatigue fracture surface in this area is linked to crack closure phenomena, which deteriorate the detection of fatigue crack.

stress intensity factor K_{cd} and the applied load F_{appl} is linear for a given crack length without crack closure phenomena. For a crack length in Region I, see Fig. 12(a), the slope of the curves is identical for the peened and unpeened material although the stress intensity factor for the peened specimen is higher as mentioned before, see e.g. Fig. 11. This observation indicates the applicability of the traditional superposition principle, implying no crack closure. In contrast, crack closure leads to a non-linear effect, see the LSP-treated specimens in Fig. 12(b) and (c). The results show, that the crack closure area that is even not connected to the crack tip changes the slope of the K_{cd} vs. F_{appl} curve, see Fig. 12(c). It is obvious, that a lower slope leads to a reduced ΔK_{cd} for given applied loads. Following the discussion in the previous section, the FCP rate is mainly influenced by ΔK_{cd} in Region II and III, a significant retardation of the FCP is only possible if the applied load range contains an area with a lower slope than present in residual stress free specimens in the K_{cd} vs. F_{appl} curve, implying the occurrence of crack closure, as observed in this study for Region II and III.

Besides the illustration of the importance of crack closure for an efficient LSP application, the K_{cd} vs. F_{appl} curves can be used for fast predictions of the FCP rate. As the K_{cd} vs. F_{appl} curves are calculated at characteristic positions of the FCP rate along the crack path, for instance the start of the peened area $a = 34$ mm and the end of the peened area $a = 49$ mm, linear relations between these

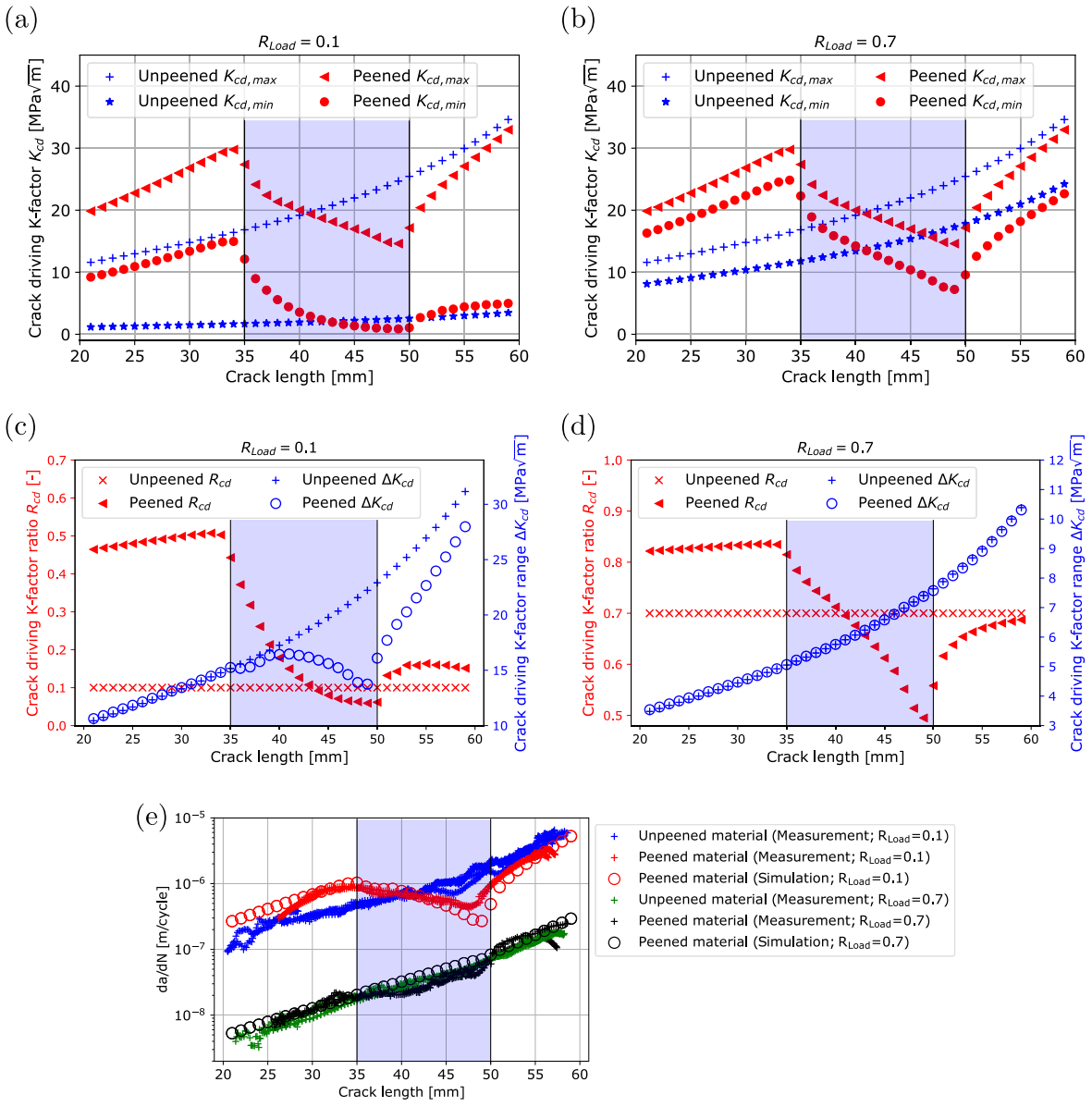

Fig. 11. Calculated crack driving stress intensity factors for unpeened and peened specimens for load ratios R_{Load} = 0.1 (a) and R_{Load} = 0.7 (b). The peened area is marked in blue. Significant differences between ΔK_{cd} of the unpeened and peened specimen are present in Regions II and III. While the significantly decreased ΔK_{cd} leads to a remarkable reduction in the FCP rate for R_{Load} = 0.1, the FCP rate is not significantly influenced by the same LSP treatment but another external loading (R_{Load} = 0.7) (e), as no significant crack closure is present. (a) is reprinted from [6], under the terms of the Creative Commons Attribution-NonCommercial-NoDerivatives 4.0 International (CC BY-NC-ND 4.0) where (c) and (e) are depicted and adopted from this reference.

points are assumed. ΔK_{cd} and R_{cd} can be directly determined from the K_{cd} vs. F_{appl} curve. Finally, just the calculation of the FCP law is needed, e.g. NASGRO equation.

In the following a short example of the application of the K_{cd} vs. F_{appl} curve to determine the effect on the FCP rate is illustrated. Assuming, the ratio of the applied forces, R_{Load}, is increased from 0.1 to 0.7, while the maximum force, 4 kN, is kept constant. This change results in a higher mean stress intensity factor at the crack tip. At the high load ratio, R_{cd} changes significantly depending on the residual stresses. In contrast, the distribution of ΔK_{cd} remain unchanged by residual stresses, see Fig. 11(d).

The latter effect can be explained by no crack closure for R_{Load} = 0.7 compared to R_{Load} = 0.1. The stress level at the minimum applied load is still high enough to keep the crack open, indicated by the same slopes of the peened and unpeened specimen in the K_{cd} vs. F_{appl} curve.

This investigation clearly reveals the importance of crack closure effects for the efficient application of LSP. The experiments show that the same LSP treatment lead to significant differences in the FCP rate retardation depending on the external loading. The

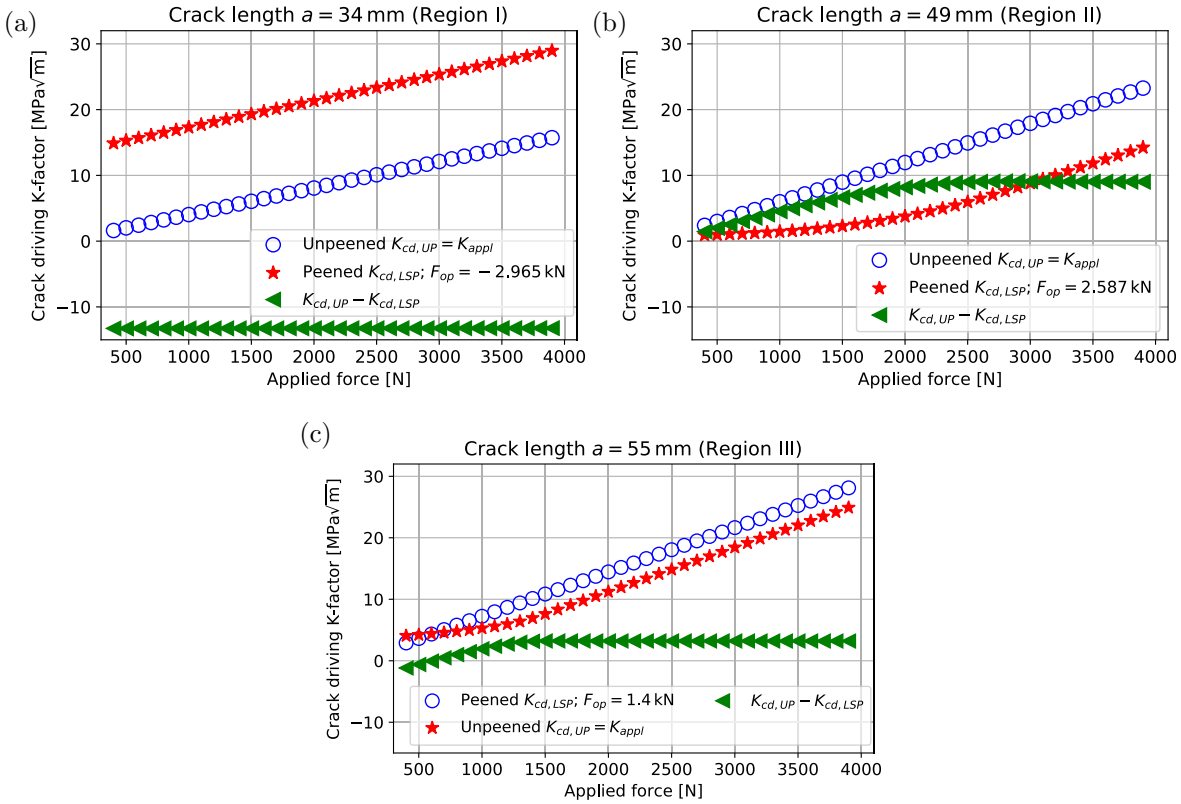

Fig. 12. Stress intensity factor K_{cd} vs. applied load F_{appl} curves exemplary for specific crack lengths in Region I–III for unpeened and peened specimens. The slope changes below F_{op}, which is related to crack closure phenomena. A significant FCP retardation is only possible if the slope of the peened material is lower than the one of the unpeened material. K_{cd} vs. F_{appl} curve allow the fast prediction of the FCP rate for arbitrary applied load cycles but the same residual stresses.

compressive residual stresses must be high enough to cause crack closure for the specific load cases to have a significant impact on the crack retardation behaviour. This finding agrees with Lados and Apelian [32], who observed the most pronounced effect of residual stresses on the FCP rate for low applied stresses, leading to a high ratio of residual to applied stresses. In case of tensile residual stresses, the stress intensity factor ratio R_{cd} is highly influenced by the tensile residual stresses if the applied loads are relatively low. Vice versa, the change of R_{cd} caused by the influence of the same tensile residual stresses is relatively low for high applied loads. This principle can be seen by the application of the traditional superposition principle, as Case 2 is present, see Section 2.3. As crack closure is found to be the main mechanism of the FCP retardation, the effect of compressive residual stresses on FCP is higher for lower applied loads, implying that crack closure is reached earlier. Additionally, these results show, that it is not only necessary to model crack closure for a precise prediction of the FCP behaviour if crack closure occurs as stated by Pavan et al. [33], crack closure is even needed for an efficient application of LSP.

5. Conclusion

The objective of this work is the investigation of the fatigue crack retardation and acceleration mechanisms in LSP-generated residual stress fields. The investigated AA2024-T3 specimens have a sheet thickness of 4.8 mm including a thin clad layer at the surfaces. FCP experiments, SEM, COD measurements, and a multi-step simulation approach are used in closed interaction to achieve a holistic explanation. Overall, the experimental and the simulation results in terms of residual stresses, FCP rate, and load vs. COD curve are in excellent agreement and lead to the following main conclusions:

- Crack closure is the main mechanism that reduces the crack driving stress intensity factor range ΔK_{cd} by changing the stress state next to the fatigue crack. The efficient application of LSP needs to cause crack closure as shown for the applied load ratio $R_{Load} = 0.1$. For $R_{Load} = 0.7$, no significant improved fatigue crack propagation behaviour is observed, as no significant amount of crack closure is present due to high minimum applied load.
- Crack closure occurs most likely in the region where compressive residual stresses are present. Furthermore, FE simulations and SEM indicated an opened crack next to the mid–thickness of the sheet, as tensile residual stresses are present in this region. The crack remains open behind the peened area during the whole load cycle if the crack tip passed the peened area, leading to a crack

closure that is not connected to the crack tip.

- Although crack closure can be measured using load vs. COD curve, a crack driving stress intensity factor is present at the crack tip. Therefore, the observation of crack closure does not indicate a zero value stress intensity factor.
- Tensile residual stresses behind the peened area do not lead to an acceleration of the fatigue crack, as crack closure in the peened area is still present, which reduces ΔK_{cd}.
- The calculation of K_{cd} vs. F_{appl} curves allow the fast prediction of FCP rates for arbitrary applied loads but given residual stresses.

Acknowledgement

The authors would like to thank the following members of the institute for their valuable work and support: Volker Ventzke for the valuable discussion on the SEM images and Hamdi Tek for the specimen preparation and performing the fatigue tests.

References

[1] Pacchinoe M, Telgkamp J. Challenges of the metallic fuselage. Proceedings 25th ICAS, Hamburg, Germany. 2006.
[2] Vaidya W, Staron P, Horstmann M. Fatigue crack propagation into the residual stress field along and perpendicular to laser beam butt-weld in aluminium alloy AA6056. Fatigue Fract Eng Mater Struct 2012;35:399–411.
[3] Peyre P, Fabbro R, Merrien P, Lieurade H. Laser shock processing of aluminium alloys. Application to high cycle fatigue behaviour. Mater Sci Eng A 1996;210:102–13.
[4] Paris P, Erdogan F. A critical analysis of crack propagation laws. J Basic Eng 1963;85:528–33.
[5] NASGRO Consortium and others, Fatigue crack growth computer program NASGRO version 3.0. user manual, JSC-22267B, NASA Technical report; 2001.
[6] Keller S, Horstmann M, Kashaev N, Klusemann B. Experimentally validated multi-step simulation strategy to predict the fatigue crack propagation rate in residual stress fields after laser shock peening. Int J Fatigue 2019;124:265–76.
[7] Fabbro R, Fournier J, Ballard P, Devaux D, Virmont J. Physical study of laser-produced plasma in confined geometry. J Appl Phys 1990;68:775–84.
[8] Chahardehi A, Brennan FP, Steuwer A. The effect of residual stresses arising from laser shock peening on fatigue crack growth. Eng Fract Mech 2010;77:2033–9.
[9] Ocaña JL, Correa C, García-Beltrán A, Porro J, Díaz M, Ruiz-de Lara L, et al. Laser shock processing of thin Al2024-T351 plates for induction of through-thickness compressive residual stresses fields. J Mater Process Technol 2015;223:8–15.
[10] Kallien Z, Keller S, Ventzke V, Kashaev N, Klusemann B. Effect of laser peening process parameters and sequences on residual stress profiles. Metals 2019;9:655.
[11] Clauer AH, Lahrman DF. Laser shock processing as a surface enhancement process. Key Eng Mater 2001;197:121–44.
[12] Verma B, Atkinson J, Kumar M. Study of fatigue behaviour of 7475 aluminium alloy. Bull Mater Sci 2001;24:231–6.
[13] Schnubel D, Huber N. The influence of crack face contact on the prediction of fatigue crack propagation in residual stress fields. Eng Fract Mech 2012;84:15–24.
[14] Servetti G, Zhang X. Predicting fatigue crack growth rate in a welded butt joint: the role of effective R ratio in accounting for residual stress effect. Eng Fract Mech 2009;76:1589–602.
[15] Parker A, factors Stress intensity, profiles crack. and fatigue crack growth rates in residual stress fields. Residual stress effects in fatigue. ASTM International; 1982.
[16] Itoh Y, Suruga S, Kashiwaya H. Prediction of fatigue crack growth rate in welding residual stress field. Eng Fract Mech 1989;33:397–407.
[17] Bao R, Zhang X, Yahaya NA. Evaluating stress intensity factors due to weld residual stresses by the weight function and finite element methods. Eng Fract Mech 2010;77:2550–66.
[18] Elber W. The significance of fatigue crack closure. Damage tolerance in aircraft structures. ASTM International; 1971.
[19] Schijve J. Fatigue of structures and materials. Springer Science & Business Media; 2001.
[20] Flügge J. The appearance of cracks and fractures in metallic materials. Düsseldorf: Verlag Stahleisen GmbH; 1997.
[21] Kerlins V, Phillips A. Modes of fracture. ASM Handbook 1987;12:12–71.
[22] Sheng J, Huang S, Zhou J, Lu J, Xu S, Zhang H. Effect of laser peening with different energies on fatigue fracture evolution of 6061–T6 aluminum alloy. Opt Laser Technol 2016;77:169–76.
[23] Sun R, Li L, Guo W, Peng P, Zhai T, Che Z, et al. Laser shock peening induced fatigue crack retardation in Ti-17 titanium alloy. Mater Sci Eng: A 2018;737:94–104.
[24] Keller S, Chupakhin S, Staron P, Maawad E, Kashaev N, Klusemann B. Experimental and numerical investigation of residual stresses in laser shock peened AA2198. J Mater Process Technol 2018;255:294–307.
[25] Johnson GR. A constitutive model and data for metals subjected to large strains, high strain rates and high temperatures. Proceedings of the 7th international symposium on ballistics. Netherlands: The Hague; 1983.
[26] Krueger R. Virtual crack closure technique: history, approach, and applications. Appl Mech Rev 2004;57:109–43.
[27] Newman JJ. A crack opening stress equation for fatigue crack growth. Int J Fract 1984;24:R131–5.
[28] Johansson S, Fitzpatrick M. Errors in crack closure measurements caused by flexure test fixture support effects. Exp Mech 2001;41:47–51.
[29] Liljedahl C, Zanellato O, Fitzpatrick M, Lin J, Edwards L. The effect of weld residual stresses and their re-distribution with crack growth during fatigue under constant amplitude loading. Int J Fatigue 2010;32:735–43.
[30] Brockman RA, Braisted WR, Olson SE, Tenaglia RD, Clauer AH, Langer K, et al. Prediction and characterization of residual stresses from laser shock peening. Int J Fatigue 2012;36:96–108.
[31] Kashaev N, Ventzke V, Horstmann M, Chupakhin S, Riekehr S, Falck R, et al. Effects of laser shock peening on the microstructure and fatigue crack propagation behaviour of thin AA2024 specimens. Int J Fatigue 2017;98:223–33.
[32] Lados DA, Apelian D. The effect of residual stress on the fatigue crack growth behavior of Al-Si-Mg cast alloys – mechanisms and corrective mathematical models. Metall Mater Trans A 2006;37:133–45.
[33] Pavan M, Furfari D, Ahmad B, Gharghouri M, Fitzpatrick ME. Fatigue crack growth in a laser shock peened residual stress field. Int J Fatigue 2019;123:157–67.